6-17-2016

An Experimental and Theoretical Study of $\tilde{A}^2A''\Pi - X^{\sim 2}A'$ Band System of the Jet-Cooled HBBr/DBBr Free Radical

Mohammed Gharaibeh
The University of Jordan, Jordan

Dennis J. Clouthier
University of Kentucky, dclaser@uky.edu

Riccardo Tarroni
Università di Bologna, Italy

An Experimental and Theoretical Study of $\tilde{A}^2A''\Pi - X^{\sim 2}A'$ Band System of the Jet-Cooled HBBr/DBBr Free Radical

Digital Object Identifier (DOI)
https://doi.org/10.1063/1.4953771

Notes/Citation Information
Published in *The Journal of Chemical Physics*, v. 144, issue 23, 234309, p. 1-11.

An experimental and theoretical study of the $\tilde{A}\,^2A'\Pi$–$\tilde{X}\,^2A'$ band system of the jet-cooled HBBr/DBBr free radical

Mohammed Gharaibeh, Dennis J. Clouthier, and Riccardo Tarroni

Citation: The Journal of Chemical Physics **144**, 234309 (2016);
View online: https://doi.org/10.1063/1.4953771
View Table of Contents: http://aip.scitation.org/toc/jcp/144/23
Published by the American Institute of Physics

An experimental and theoretical study of the $\tilde{A}^2A''\Pi$–$\tilde{X}^2A'$ band system of the jet-cooled HBBr/DBBr free radical

Mohammed Gharaibeh,[1] Dennis J. Clouthier,[2,a)] and Riccardo Tarroni[3]
[1]*Department of Chemistry, The University of Jordan, Amman 11942, Jordan*
[2]*Department of Chemistry, University of Kentucky, Lexington, Kentucky 40506–0055, USA*
[3]*Dipartimento di Chimica Industriale "Toso Montanari," Università di Bologna, Viale Risorgimento 4, 40136 Bologna, Italy*

(Received 30 March 2016; accepted 31 May 2016; published online 17 June 2016)

The electronic spectra of the HBBr and DBBr free radicals have been studied in depth. These species were prepared in a pulsed electric discharge jet using a precursor mixture of BBr_3 vapor and H_2 or D_2 in high pressure argon. Transitions to the electronic excited state of the jet-cooled radicals were probed with laser-induced fluorescence and the ground state energy levels were measured from the single vibronic level emission spectra. HBBr has an extensive band system in the red which involves a linear-bent transition between the two Renner-Teller components of what would be a $^2\Pi$ state at linearity. We have used high level *ab initio* theory to calculate potential energy surfaces for the bent $^2A'$ ground state and the linear $\tilde{A}^2A''\Pi$ excited state and we have determined the ro-vibronic energy levels variationally, including spin orbit effects. The correspondence between the computed and experimentally observed transition frequencies, upper state level symmetries, and H and B isotope shifts was used to make reliable assignments. We have shown that the ground state barriers to linearity, which range from 10 000 cm^{-1} in HBF to 2700 cm^{-1} in BH_2, are inversely related to the energy of the first excited $^2\Sigma$ ($^2A'$) electronic state. This suggests that a vibronic coupling mechanism is responsible for the nonlinear equilibrium geometries of the ground states of the HBX free radicals. *Published by AIP Publishing.* [http://dx.doi.org/10.1063/1.4953771]

I. INTRODUCTION

The boron trihalides BF_3, BCl_3, BBr_3, and BI_3 have been extensively used as boron sources in the chemical vapor deposition (CVD) production of boron carbide and boron nitride, materials that, after diamond, are among the hardest known. Although BCl_3 is the most commonly used boron source in such processes, it has the disadvantages of being corrosive and difficult to handle and requiring relatively high temperatures (1200–2000 °C) to obtain crystalline materials.[1,2] Based on a thermodynamic study, it has been suggested[3] that BBr_3 should be a much better CVD boron source, with the added advantage of easier handling and storage. Subsequent work has shown that boron tribromide is a safe and efficient precursor for the plasma-assisted CVD synthesis of high quality boron coatings using BBr_3—CH_4—H_2 gas mixtures.[4] Similarly, well crystallized and highly dense films of boron nitride have been produced at moderate temperatures by low pressure CVD using BBr_3—NH_3—H_2 precursor gas mixtures.[5]

There has been little work on the detailed mechanisms of CVD processes involving BBr_3—H_2 mixtures and the relevant reactive intermediates are unknown. However, analogy to experimental[6–8] and theoretical studies[9–12] of the corresponding BCl_3—H_2 systems suggests that the BBr, BBr_2, BH_2, BH, and HBBr free radicals should be important in these processes. All of these species have been spectroscopically characterized with the exception of HBBr which is the subject of the present work.

In 2005, we reported that the HBF, HBCl, and HBBr free radicals were viable gas phase species that could be synthesized from BX_3/H_2 mixtures in a pulsed discharge jet and detected by laser-induced fluorescence (LIF) techniques.[13] In each case, the free radical has an extensive band system in the red which involves a linear-bent transition between the two Renner-Teller components of what would be a $^2\Pi$ state at linearity. Since the 0_0^0 band occurs at very low energies in the near-infrared and the observed bands terminate on quite high bending levels in the excited state, the detailed assignment of the vibrational structure in the LIF spectra is challenging. In a previous work on HBF/DBF[14,15] and HBCl/DBCl,[16] we have used a combined theoretical and experimental approach to tackle the problem. In each case, we first used a high level *ab initio* theory to calculate a suitable grid of points on the ground and excited state potential energy surfaces. Then we employed the variational methods developed by Carter and co-workers[17,18] to obtain the ground and excited state ro-vibronic energy levels from the fitted potentials, including the effects of spin-orbit and Renner-Teller couplings. Finally, we used the theoretical predictions of the vibrational energy levels and the boron, hydrogen, and halogen (where applicable) isotope effects to make assignments of the vibrational bands in the observed spectra. We now conclude these studies with a similar investigation of the electronic spectrum of the HBBr free radical.

a)Author to whom correspondence should be addressed. Electronic mail: dclaser@uky.edu.

II. EXPERIMENT

The HBBr or DBBr free radicals were generated by seeding the vapor of liquid boron tribromide into a mixture of 40 psi of argon diluted with 5% H_2 or D_2 and subjecting pulses of this gas mixture to an electric discharge. As described in detail elsewhere,[19,20] a pulsed molecular beam valve (General Valve, series 9) injected the precursor mixture into a flow channel where an electric discharge between two stainless steel ring electrodes fragmented it, producing the radical of interest. The reactive intermediates were rotationally and vibrationally cooled by free jet expansion into vacuum at the exit of the pulsed discharge apparatus. A 1.0 cm long reheat tube[21] added to the end of the discharge apparatus increased production of the species of interest and suppressed the background glow from excited argon atoms.

Low resolution (0.1 cm^{-1}) survey LIF spectra were recorded using a Nd:YAG or excimer pumped dye laser (Lumonics HD-300) excitation source. The fluorescence was collected by a lens, focused through appropriate longwave pass filters, and onto the photocathode of a photomultiplier tube (EMI 9816QB). The spectra were calibrated with optogalvanic lines from various argon- and neon-filled hollow cathode lamps to an estimated accuracy of 0.1 cm^{-1}. The laser-induced fluorescence and calibration spectra were digitized and recorded simultaneously on a LabVIEW-based data acquisition system.

For emission spectroscopy, previously measured LIF band maxima in the spectra of HBBr and DBBr were excited by the dye laser and the resulting fluorescence was imaged with $f/1.5$ optics onto the entrance slit of a 0.5 m scanning monochromator (Spex 500M). The pulsed fluorescence signals were detected with a cooled, red-sensitive photomultiplier (RCA C31034A), amplified, processed using a gated integrator and recorded digitally. The emission spectra were calibrated to an estimated accuracy of ±3 cm^{-1} using emission lines from an argon lamp. A 1200 line/mm grating blazed at 750 nm was employed in this work, with a bandpass of 0.6–0.8 nm, depending on the signal intensity.

The broadband LIF spectra were generally of low quality because of fluorescence of impurity species, formed in the discharge along with HBBr or DBBr, which overlapped the emission of the target radical, and the overall weakness of the emission. The synchronous scan LIF (sync-scan LIF) technique[22] was employed to filter out the unwanted emission and detect only fluorescence from the species of interest. This method utilizes the emission monochromator as a narrow band pass filter which is scanned synchronously with the laser, keeping a constant offset from the laser frequency. The offset (in cm^{-1}) value is a vibrational interval of the ground state of the molecule of interest determined from the emission spectrum. By using sync-scan LIF, we were able to get better and cleaner, although still quite weak spectra of HBBr and DBBr.

III. RESULTS AND ANALYSIS

A. Preliminary *ab initio* calculations

In a preliminary stage of the work, we have used the Gaussian 03 program[23] package to predict the properties of the ground and excited states of HBBr and its various isotopologues with both density functional theory (DFT) with the Becke three parameter hybrid density functional[24] and the Lee, Yang, and Parr correlation functional[25] [B3LYP], and at the coupled cluster singles and doubles with perturbative triples [CCSD(T)] level of theory.[26] In both cases, we employed Dunning's correlation-consistent triple-zeta basis set augmented by diffuse functions (aug-cc-pVTZ)[27] as a reasonable compromise between accuracy and computational expense. The resulting molecular geometries, excited state T_e, and the vibrational frequencies are summarized in Table I.

Both theoretical methods predict that HBBr is a bent molecule in the ground state with the electron configuration

$$[\text{core}]\ (12a')^2(13a')^2(14a')^2(5a'')^2(15a')^2(16a')^1(6a'')^0\ \tilde{X}^2A',$$

where the $16a'$ (HOMO) and $6a''$ (LUMO) are the in- and out-of-plane BBr π antibonding orbitals. Promotion of an electron from the HOMO to the LUMO (which is predominantly an out-of-plane $2p_z$ boron orbital) produces the linear first excited state which is symbolized using the notation of Dressler and

TABLE I. *Ab initio* predictions [CCSD(T) with B3LYP in parentheses] of the ground and first excited state vibrational frequencies of the various isotopologues of HBBr. All quantities are in cm^{-1}.

	$\tilde{X}^2A'$			$\tilde{A}^2A''\Pi$		
	ω_1	ω_2	ω_3	ω_1	ω_2	ω_3
$H^{11}B^{79}Br$	2656 (2650)[a,b,c]	845 (832)	725 (705)	2845 (2853)	674 (663)	791 (773)
$H^{11}B^{81}Br$	2656 (2650)	845 (832)	724 (704)	2845 (2853)	674 (663)	790 (772)
$H^{10}B^{79}Br$	2667 (2661)	857 (842)	749 (729)	2859 (2867)	681 (670)	821 (803)
$H^{10}B^{81}Br$	2656 (2661)	845 (842)	724 (728)	2859 (2867)	681 (670)	820 (801)
$D^{11}B^{79}Br$	1960 (1956)	602 (594)	748 (726)	2116 (2120)	523 (514)	757 (740)
$D^{11}B^{81}Br$	1961 (1956)	602 (594)	748 (725)	2116 (2121)	523 (514)	755 (739)
$D^{10}B^{79}Br$	1977 (1972)	608 (600)	778 (755)	2137 (2142)	531 (522)	781 (764)
$D^{10}B^{81}Br$	1977 (1972)	607 (599)	777 (754)	2137 (2142)	531 (522)	780 (763)

[a]Both calculations with an aug-cc-pVTZ basis set. Using standard notation, ω_1 = BH stretch, ω_2 = bend, and ω_3 = BBr stretch. The excited state imaginary bending frequency was discarded.
[b]The geometric parameters are r''(BH) = 1.1894 (1.1867) Å, r''(BBr) = 1.8728 (1.8785) Å, θ''(HBBr) = 123.77 (123.75)°, r'(BH) = 1.1695 (1.1657) Å, r'(BBr) = 1.8317 (1.8353) Å, and θ'(HBBr) = 180°.
[c]Excited state T_e = 5464 (5042) cm^{-1}.

Ramsay[28] as $\tilde{A}^2A''\Pi$, to denote the fact that it is the upper C_s component of a Renner-Teller pair of states. Although the bond angle increases by more than 56° on electronic excitation, the bond lengths actually decrease by a few hundredths of an angstrom, consistent with the notion that excitation is from an in-plane antibonding orbital to an out-of-plane orbital largely localized on the central boron atom. A corresponding increase in the frequencies of the stretching vibrations is evident in the results presented in Table I. The results are in excellent agreement with previously published[29] larger basis set CCSD(T) calculations of the ground state properties of $HB^{79}Br$.

B. Potential energy surface calculations

All single point energy calculations were performed with the Cfour suite of quantum chemistry programs.[30] Single point energies of the bent $\tilde{X}^2A'$ ground state and the linear $\tilde{A}^2A''\Pi$ first excited state were calculated at the CCSD(T) level of theory[26] with the cc-pVQZ,[27] cc-pwCVQZ,[31] and cc-pwCVQZ-PP[32] basis sets for hydrogen, boron, and bromine, respectively, using unrestricted Hartree-Fock wavefunctions with the proper symmetry as references. All electrons were correlated. The geometries of the single point calculations were carefully chosen in order to properly map the potential energy surfaces (PES) of the ground and of the excited states for energies up to 20 000 cm^{-1} above their respective minima. The geometries were in the ranges $2.9 \le r_{BBr} \le 4.7$ bohr and $1.7 \le r_{BH} \le 3.3$ bohr for the stretching coordinates (both states) and $70 \le \theta_{HBBr} \le 180$ ($\tilde{X}^2A'$ state, 836 points) and $100 \le \theta_{HBBr} \le 180$ ($\tilde{A}^2A''\Pi$ state, 672 points).

In the variational Renner-Teller calculations (see below), the fully *ab initio* PESs yielded vibronic $\tilde{A}^2A''$ state levels, which were ~100 cm^{-1} too high for the main bands of the spectra. Similar deviations were observed also for HBF[14] and HBCl,[16] which lead to errors of ~2% in the corresponding barrier to linearity in the lower electronic state. For these two radicals, these approximately constant shifts did not constitute an obstacle to the assignment of the experimental bands, thanks to the comparatively simpler structure of the observed transitions. However HBBr has a much more complex spectrum, which persuaded us to introduce an empirical correction to the *ab initio* surfaces, in order to facilitate the assignment of the weaker features. In order to improve the agreement between theory and experiment, the *ab initio* energies have been modified in the following way. For the $\tilde{A}^2A''$ state, all the energies were uniformly shifted downwards by 0.000 447 hartree (98 cm^{-1}). For the $\tilde{X}^2A'$ state, the energies for geometries with bond angles of 180° were decreased by the same amount, and all the geometries with bending angle $\theta_{HBBr} = 170°$ and $\theta_{HBBr} = 160°$ were discarded from the fit.

The modified energies of the two states were fitted with the SURFIT program,[33] using symmetry restricted polynomial functions with the general form

$$V^{\eta}(q_1,q_2,q_3) = \sum_{ijk} c^{\eta}_{ijk}(q_1 - q_1^{ref,\eta})^i(q_2 - q_2^{ref,\eta})^j \times (q_3 - q_3^{ref,\eta})^k, \quad (1)$$

where η refers to the specific electronic state, $q_1 = r_{BBr}$ stretching, $q_2 = r_{BH}$ stretching, and $q_3 = \theta_{HBBr}$ bending, and $q_1^{ref,\eta}$, $q_2^{ref,\eta}$, $q_3^{ref,\eta}$ defines the reference geometry of the η-th state. Symmetry restrictions constrain k to be even for the $\tilde{A}^2A''$ state. The two PESs have been expanded at their computed equilibrium geometries and the fitting coefficients c^{η}_{ijk} are presented as the supplementary material.[34] The root mean square deviation (RMSD) of the least squares fitting was 4.7 cm^{-1} and 2.6 cm^{-1} for the $\tilde{X}^2A'$ and $\tilde{A}^2A''$ states, respectively. The degeneracy of the two surfaces at linearity was imposed by using 52 linear geometries in the fitting of the ground state coefficients. This procedure is identical to that adopted for HBCl[16] and it is able to recover surfaces which are nearly degenerate for linear geometries, with differences of the same order of magnitude of the RMSD's of the fittings. From the fitted surfaces, the barrier to linearity of the ground state was calculated to be 5607 cm^{-1}, slightly lower than the 6073 cm^{-1} value found for HBCl,[16] but much lower than the 10 084 cm^{-1} value found for HBF.[14] Potential energy curves as a function of bond angle for fixed bond lengths, illustrating the nature of the relevant electronic states, are shown in Fig. 1.

Using the Molpro2010 code,[35] the geometry independent phenomenological spin-orbit splitting of the electronic Π ($\tilde{X}^2A'$, $\tilde{A}^2A''$) state at its linear equilibrium geometry was calculated to be 299.7 cm^{-1}, at the CASSCF level of theory using the cc-pVQZ[27] basis set for all atoms. This value is substantially larger than that calculated for HBCl[16] (87.3 cm^{-1}) and HBF[14] (42.3 cm^{-1}).

C. Calculation of the vibronic energy levels

The analytically fitted surfaces were used for the variational calculation of the rovibronic energy levels. For this purpose, we used the code originally developed by Carter and co-workers[17] because of the problems found[36] in the RVIB3 program[18] when linear-bent Renner-Teller cases are handled.

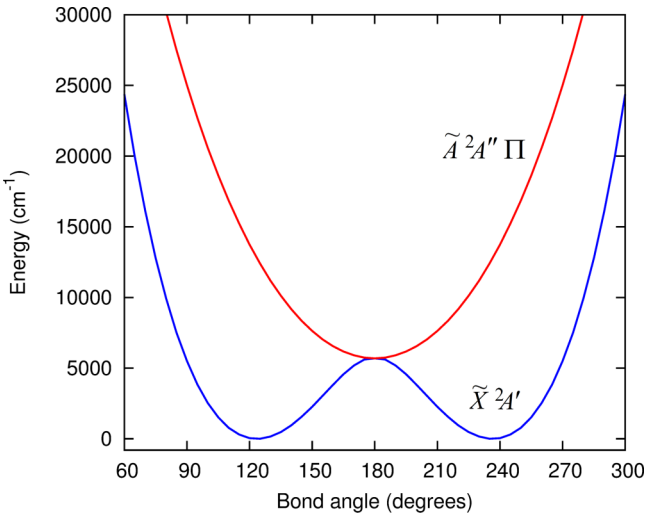

FIG. 1. Potential energy curves in the absence of spin-orbit effects as a function of the bond angle coordinate for the $\tilde{X}^2A'$ and $\tilde{A}^2A''$ states of HBBr. The bond lengths are fixed at the ground state equilibrium values (r_{BH} = 1.186 Å and r_{BBr} = 1.863 Å).

The variational basis set was built from 20 to 30 harmonic oscillators for the BH and BBr stretches, respectively, and 104 Legendre polynomials for the bend of the two electronic states, contracted to 81 two-dimensional stretching functions and 54 two dimensional bending functions. Spin-rovibronic calculations for $J = {}^1/_2, {}^3/_2, {}^5/_2, {}^7/_2$, were performed with the inclusion of the spin-orbit effect, thus enabling the prediction of the energies and spin-orbit splittings for levels with $K \leq 3$ (Σ, Π, Δ, Φ levels). The vibrational quantum numbers were assigned by inspection of the variational coefficients and, for higher levels, by counting the nodes in plots of the vibrational wavefunctions. All eight isotopologues ($H^{11}B^{79}Br$, $H^{10}B^{79}Br$, $H^{11}B^{81}Br$, $H^{10}B^{81}Br$, $D^{11}B^{79}Br$, $D^{10}B^{79}Br$, $D^{11}B^{81}Br$, and $D^{10}B^{81}Br$) were studied, for energies up to 20 000 cm^{-1} above the $\tilde{X}^2A'$ (0,0,0) level.

The resulting calculated values for the low-lying ground state vibrational energy levels of the eight isotopologues are given in Table II. In Table III, we show the calculated excited state energy levels, for (0,v_2,0), (1,v_2,0), and (0,v_2,1) sequences, relative to the ground state $\tilde{X}^2A'(0,0,0)$ energy level. Only Σ and Π states are included in Table III, since only these states proved to be relevant for the interpretation of the spectra.

D. LIF spectra

The sync-scan LIF method eliminated many of the extraneous bands in the spectra and allowed precise measurements and definitive assignments to be made, as will be discussed later. Fig. 2 illustrates the sync-scan LIF spectrum of $H^{11}BBr$ in the range from 13 500 to 17 500 cm^{-1}. In this instance, the sync-scan offset was set to 835 cm^{-1}, which our emission spectra (see below) and the PES calculations (above) show as one quantum of the ground state bending frequency. A simple progression of bands with an interval of about 600–650 cm^{-1} is clearly evident along with a variety of weaker features. The $\Delta K = \pm 1$ selection rule, and experience with the spectra of HBF and HBCl, suggest that if these are cold band transitions, they originate from the $K_a'' = 0$, 1, or 2 levels and terminate on the $K = 1(\Pi)$, $K = 0(\Sigma)$ or $K = 2(\Delta)$, or $K = 1(\Pi)$ or $K = 3(\Phi)$ excited state levels, respectively. Before we discuss the details of the assignments, it is necessary to examine the SVL emission spectra obtained by laser excitation of the prominent bands in the LIF spectra, as they contain information that is important for the analysis of the LIF spectra.

E. Emission spectra

The emission spectra obtained for HBBr and especially DBBr were generally quite weak and noisy, so reliable measurements were only obtained for a few bands in each instance. Some of the better examples are shown in Fig. 3. The top panel shows the spectrum obtained by laser excitation of the Q-branch maximum of the $H^{11}BBr$ band at 18 031 cm^{-1}. The spectrum is dominated by a single progression with an interval of 839–802 cm^{-1} which can be readily identified from the data in Table II as the bending mode. In this case, the upper state must have $K = 0$ (Σ state) as the $\Delta K = \pm 1$ selection rule mandates that only transitions down to $K_a'' = 1$ can occur, so

TABLE II. Calculated $\tilde{X}^2A'$ state vibronic levels of the HBBr isotopologues (in cm^{-1}).

(v_1,v_2,v_3)	$H^{11}B^{79}Br$	$H^{10}B^{79}Br$	$H^{11}B^{81}Br$	$H^{10}B^{81}Br$	$D^{11}B^{79}Br$	$D^{10}B^{79}Br$	$D^{11}B^{81}Br$	$D^{10}B^{81}Br$
(0,0,1)	717.7	740.8	716.6	739.8	742.4	771.1	741.6	770.2
(0,1,0)	838.1	849.4	838.1	849.3	599.0	604.3	598.6	603.9
(0,0,2)	1429.0	1475.4	1426.7	1473.3	1475.7	1532.0	1474.0	1530.3
(0,1,1)	1554.8	1588.5	1553.6	1587.3	1334.2	1367.7	1333.0	1366.5
(0,2,0)	1660.9	1682.7	1660.8	1682.4	1196.3	1206.8	1195.5	1206.1
(0,0,3)	2133.6	2203.5	2130.3	2200.4	2200.3	2283.4	2197.8	2280.9
(0,1,2)	2264.8	2321.5	2262.5	2319.3	2060.5	2121.3	2058.4	2119.3
(0,2,1)	2376.5	2419.7	2375.3	2418.4	1924.7	1962.6	1923.2	1961.1
(0,3,0)	2466.3	2498.2	2466.1	2497.8	1791.7	1807.4	1790.5	1806.3
(1,0,0)	2558.6	2569.5	2558.6	2569.5	1909.5	1925.9	1909.4	1925.9
(0,0,4)	2831.6	2925.0	2827.2	2920.9	2916.5	3025.6	2913.2	3022.3
(0,1,3)	2968.3	3048.2	2964.9	3045.0	2778.3	2865.5	2775.4	2862.7
(0,2,2)	3085.6	3151.0	3083.3	3148.8	2640.9	2711.3	2638.6	2709.3
(0,3,1)	3181.1	3232.2	3179.8	3231.0	2514.3	2555.5	2512.7	2553.7
(0,4,0)	3252.3	3294.7	3252.0	3294.1	2384.5	2405.3	2383.0	2403.9
(1,0,1)	3273.5	3306.1	3272.4	3305.1	2658.0	2698.4	2657.0	2697.1
(1,1,0)	3391.0	3414.9	3390.9	3414.7	2499.5	2522.6	2498.7	2522.2
(0,0,5)	3522.9	3639.7	3517.5	3634.5	3624.7	3758.9	3620.4	3754.8
(0,1,4)	3665.0	3768.2	3660.5	3764.0	3488.0	3590.3	3484.2	3588.5
(0,2,3)	3788.0	3876.3	3784.6	3873.1	3352.1	3442.3	3348.8	3439.2
(0,3,2)	3889.0	3961.6	3887.1	3959.4	3217.9	3281.3	3215.3	3279.3
(0,4,1)	3966.5	4024.3	3965.1	4023.0	3103.6	3146.4	3102.0	3144.4
(1,0,2)	3982.2	4036.9	3980.0	4034.9	3393.0	3467.7	3391.3	3465.9
(0,5,0)	4017.6	4072.5	4017.3	4071.5	2974.1	2999.9	2972.4	2998.3
(1,1,1)	4104.6	4149.3	4103.4	4148.2	3245.0	3301.5	3243.5	3299.5

TABLE III. Calculated $\tilde{A}^2A''$ state vibronic levels of HBBr isotopologues (in cm^{-1}). For Π levels, the average of the four spin and K components is reported. The spin-orbit splittings of the Π levels, calculated as (K-averaged) $\Pi_{3/2}-\Pi_{1/2}$ differences, are given in parentheses.

(v_1,v_2,v_3)	$H^{11}B^{79}Br$	$H^{10}B^{79}Br$	$H^{11}B^{81}Br$	$H^{10}B^{81}Br$	$D^{11}B^{79}Br$	$D^{10}B^{79}Br$	$D^{11}B^{81}Br$	$D^{10}B^{81}Br$
(0,1,0)Σ	6 533.7	6 546.2	6 533.6	6 546.0	6 319.1	6 335.8	6 318.7	6 335.2
(0,2,0)Π	7 115.2 (5.0)	7 139.8 (3.8)	7 114.8 (−5.4)	7 139.6 (3.6)	6 781.8 (−59.9)	6 791.6 (−48.7)	6 779.3 (−60.3)	6 789.5 (−49.0)
(0,3,0)Σ	7 820.8	7 848.3	7 820.5	7 848.1	7 340.5	7 365.3	7 339.4	7 364.1
(0,4,0)Π	8 487.4 (46.7)	8 527.5 (56.9)	8 487.1 (46.7)	8 527.2 (56.0)	7 829.9 (8.6)	7 865.0 (7.4)	7 828.1 (6.2)	7 862.6 (7.1)
(0,5,0)Σ	9 135.8	9173.1	9 135.5	9 172.9	8 358.0	8 401.7	8 356.5	8 400.6
(0,6,0)Π	9 763.5 (−11.8)	9 813.9 (4.0)	9 762.9 (−12.4)	9 813.2 (3.7)	8 873.2 (40.3)	8 953.9 (65.9)	8 871.0 (37.2)	8 949.6 (66.3)
(0,7,0)Σ	10 432.5	10 466.8	10 432.1	10 465.7	9 372.9	9 444.8	9 371.6	9 443.2
(0,8,0)Π	11 097.4 (40.3)	11 166.4 (48.0)	11 096.7 (40.4)	11 165.5 (47.2)	9 874.7 (−3.4)	9 959.4 (12.5)	9 873.0 (−5.1)	9 957.0 (8.9)
(0,9,0)Σ	11 723.4	11 785.7	11 722.8	11 785.3	10 376.7	10 481.0	10 375.0	10 479.2
(0,10,0)Π	12 356.0 (−7.6)	12 426.0 (−2.6)	12 355.6 (−7.6)	12 426.4 (−2.6)	10 896.3 (1.7)	10 993.1 (2.0)	10 894.8 (−3.0)	10 993.4 (−3.3)
(0,11,0)Σ	12 415.7	13 081.1	12 414.8	13 080.5	11 411.0	11 510.8	11 410.1	11 506.6
(0,12,0)Π	13 643.8 (2.8)	13 730.0 (12.7)	13 643.2 (2.5)	13 728.6 (11.1)	11 912.5 (−1.8)	12 022.1 (−12.3)	11 910.1 (−4.9)	12 019.6 (−17.3)
(0,13,0)Σ	14 271.3	14 362.0	14 270.6	14 361.1	12 430.2	12 552.8	12 426.2	12 549.2
(0,14,0)Π	14 919.4 (4.8)	15 014.2 (10.3)	14 918.7 (4.5)	15 013.6 (10.2)	12 932.4 (10.4)	13 063.8 (2.0)	12 930.0 (7.9)	13 062.2 (0.8)
(0,15,0)Σ	15 550.3	15 648.4	15 549.6	15 647.7	13 442.5	13 579.7	13 438.8	13 576.6
(0,16,0)Π	16 185.6 (7.5)	16 288.5 (7.4)	16 184.2 (5.7)	16 288.6 (7.0)	13 941.6 (8.9)	14 093.2 (0.1)	13 939.0 (6.1)	14 090.1 (−3.4)
(0,17,0)Σ	16 808.0	16 917.2	16 807.5	16 916.3	14 442.2	14 608.9	14 438.8	14 604.4
(0,18,0)Π	17 438.5 (0.3)	17 554.2 (7.6)	17 437.7 (0.0)	17 552.3 (4.7)	14 948.5 (10.4	15 120.7 (2..8)	14 945.4 (6.9)	15 120.3 (5-0)
(0,19,0)Σ	18 071.4	18 193.5	18 070.4	18 194.3	15 442.3	15 631.5	15 438.6	15 625.0
(0,20,0)Π	18 686.0 (3.4)	18 806.6 (10.5)	18 686.3 (6.2)	18 805.2 (9.6)	15 949.6 (8.9)	16 142.0 (1.6)	15 950.2 (13.1)	16 140.5 (1.5)
(0,21,0)Σ	19 296.6	19 420.6	19 295.5	19 419.9	16 437.8	16 652.9	16 431.2	16 650.4
(0,22,0)Π	19 913.3 (1.0)	20 069.5 (3.1)	19 940.3 (−2.5)	20 068.3 (2.6)	16 944.8 (5.4)	17 159.5 (2.2)	16 945.0 (9.3)	17 156.5 (−0.2)
(0,23,0)Σ					17 443.3	17 669.8	17 440.5	17 665.6
(0,24,0)Π					17 935.0 (0.7)	18 172.6 (3.8)	17 935.3 (5.0)	18 169.2 (1.0)
(0,25,0)Σ					18 429.5	18 677.6	18 427.4	18 674.1
(0,26,0)Π					18 916.2 (−11.2)	19 175.3 (−4.8)	18 914.1 (−11.4)	19 171.9 (−8.4)
(0,1,1)Σ	7 310.1	7 350.7	7 308.7	7 349.4	7 059.7	7 118.8	7 056.9	7 115.2
(0,2,1)Π	7 876.6 (−14.9)	7 929.4 (−2.8)	7 875.1 (−14.9)	7 927.9 (−3.0)	7 524.7 (6.0)	7 570.4 (11.2)	7 522.3 (6.3)	7 566.7 (9.0)
(0,3,1)Σ	8 632.2	8 704.1	8 630.6	8 702.0	8 083.9	8 130.4	8 080.3	8 127.5
(0,4,1)Π	9 249.7 (49.8)	9 314.6 (55.2)	9 248.4 (49.9)	9 313.3 (55.4)	8 526.9 (−58.8)	8 600.4 (−52.3)	8 522.9 (−60.2)	8 596.1 (−54.4)
(0,5,1)Σ	9 904.0	9 969.6	9 902.5	9 968.1	9 088.9	9 159.9	9 086.7	9 157.9
(0,6,1)Π	10 519.8 (−27.5)	10 596.6 (−16.7)	10 518.1 (−27.7)	10 594.8 (−17.2)	9 568.3 (−15.7)	9 659.6 (4.0)	9 564.8 (−14.8)	9 657.1 (2.9)
(0,7,1)Σ	11 193.0	11 277.5	11 191.4	11 274.9	10 102.7	10 174.9	10 099.2	10 172.5
(0,8,1)Π	11 839.0 (11.3)	11 928.3(22.1)	11 837.2 (11.4)	11 926.6 (22.0)	10 599.6 (11.1)	10 683.2 (−16.5)	10 595.7 (8.4)	10 679.1 (−17.2)
(0,9,1)Σ	12 483.0	12 574.7	12 481.2	12 571.9	11 121.3	11 219.1	11 116.2	11 216.1
(0,10,1)Π	13 120.4 (5.6)	13 213.6 (2.9)	13 118.2 (5.4)	13 211.6 (2.2)	11 606.8 (−8.4)	11 721.2 (−7.6)	11 604.9 (−12.7)	11 717.4 (−9.9)
(0,11,1)Σ	13 749.1	13 858.6	13 744.7	13 856.9	12 126.9	12 249.5	12 120.1	12 246.5
(0,12,1)Π	14 396.1 (0.6)	14 505.2 (3.9)	14 394.8 (2.5)	14 503.1 (3.7)	12 619.7 (−5.4)	12 761.3 (12.9)	12 615.4 (−9.8)	12 759.1 (13.1)
(0,13,1)Σ	15 034.5	15 155.3	15 032.8	15 151.9	13 141.3	13 276.1	13 135.9	13 272.0
(0,14,1)Π	15 657.4 (−16.0)	15 779.4 (−8.0)	15 655.9 (−14.8)	15 777.8 (−7.7)	13 633.7 (7.4)	13 775.7 (−10.9)	13 629.0 (4.3)	13 768.9 (−20.3)
(0,15,1)Σ	16 299.2	16 420.8	16 297.1	16 418.9	14 146.9	14 298.2	14 141.5	14 295.8
(0,16,1)Π	16 922.6 (−8.7)	17 053.1 (−5.6)	16 921.2 (−7.6)	17 051.1 (−6.0)	14 635.2 (3.7)	14 807.6 (7.6)	14 630.8 (−0.3)	14 805.9 (8.8)
(0,17,1)Σ	17 557.9	17 696.3	17 554.9	17 693.5	15 134.0	15 315.8	15 130.9	15 312.2
(0,18,1)Π	18 179.5 (−0.6)	18 317.9 (−1.9)	18 177.3 (−1.0)	18 315.7 (−2.1)	15 626.9 (−11.3)	15 820.5 (−4.3)	15 623.5 (−14.2)	15 815.6 (−9.2)
(0,19,1)Σ	18 801.6	18 945.5	18 799.5	18 943.5	16 134.0	16 341.7	16 130.7	16 335.7
(0,20,1)Π	19 430.7 (13.2)	19 571.3 (10.5)	19 426.8 (15.1)	19 568.4 (8.5)	16 629.8 (3.2)	16 836.3 (−1.7)	16 627.3 (3.0)	16 832.9 (−3.2)
(0,21,1)Σ	20 039.0	20 186.3	20 036.1	20 184.2	17 127.8	17 346.9	17 124.3	17 343.7
(0,22,1)Π					17 619.9 (1.7)	17 846.5 (−0.8)	17 615.0 (−2.5)	17 841.9 (−4.4)
(0,23,1)Σ					18 112.0	18 347.7	18 107.3	1 8340.2
(1,1,0)Σ	9 267.3	9 292.3	9 267.1	9 292.2	8 375.9	8 416.7	8 374.1	8 415.0
(1,2,0)Π	9 824.3 (−52.5)	9 870.2 (−15.7)	9 823.9 (−52.7)	9 869.3 (−16.1)	8 831.1(25.1)	8 896.3 (34.0)	8 827.4 (25.0)	8 892.7 (34.4)
(1,3,0)Σ	10 546.0	10 586.6	10 545.7	10 586.3	9 396.9	9 430.1	9 394.2	9 429.5
(1,4,0)Π	11 173.4 (19.6)	11 227.8 (28.2)	11 173.0 (19.2)	11 226.3 (29.3)	98 56.7 (0.5)	9 913.0 (−24.0)	9 854.3 (−1.4)	9 910.3 (−25.1)
(1,5,0)Σ	11 809.6	11 860.4	11 809.2	11 859.5	10 374.5	10 445.8	10 371.8	10 443.9
(1,6,0)Π	12 408.1 (−53.2)	12 477.1 (−35.7)	12 406.4 (−55.8)	12 476.4 (−35.4)	10 880.7 (17.7)	10 959.3 (24.0)	10 878.6 (13.2)	10 955.0 (19.9)
(1,7,0)Σ	13 090.4	13 153.6	13 090.0	13 153.3	11 389.9	11 472.9	11 388.2	11 469.8
(1,8,0)Π	13 705.2 (−12.5)	13 775.9 (−7.7)	13 704.8 (−12.6)	13 775.5 (−7.8)	11 883.4 (10.3)	11 979.8 (10.2)	11 880.4 (6.4)	11 973.1 (−1.7)
(1,9,0)Σ	14 351.1	14 432.3	14 350.6	14 431.4	12 388.6	12 490.3	12 387.4	12 486.6
(1,10,0)Π	14 955.7 (−19.4)	15 046.6 (−12.7)	14 953.4 (−20.7)	15 045.1 (−13.0)	12 881.9 (−1.4)	12 998.9 (−0.1)	12 879.7 (−4.4)	12 997.1 (−0.9)

TABLE III. (*Continued.*)

(υ_1,υ_2,υ_3)	$H^{11}B^{79}Br$	$H^{10}B^{79}Br$	$H^{11}B^{81}Br$	$H^{10}B^{81}Br$	$D^{11}B^{79}Br$	$D^{10}B^{79}Br$	$D^{11}B^{81}Br$	$D^{10}B^{81}Br$
(1,11,0)Σ	15 601.8	15 690.0	15 600.9	15 689.4	13 398.3	13 512.3	13 392.2	13 509.8
(1,12,0)Π	16 230.0 (0.3)	16 324.2 (2.9)	16 228.7 (−1.3)	16 323.5 (2.8)	13 889.8 (9.7)	14 030.5 (20.2)	13 887.5 (6.7)	14 026.8 (13.6)
(1,13,0)Σ	16 853.0	16 951.7	16 852.0	16 949.9	14 395.4	14 533.5	14 391.3	14 530.1
(1,14,0)Π	17 477.0 (12.6)	17 583.4 (15.5)	17 474.0 (14.4)	17 583.6 (12.6)	14 875.7 (−16.2)	15 036.8 (−4.0)	14 873.8 (−18.5)	15 035.1 (−6.7)
(1,15,0)Σ	18 093.4	18 204.5	18 092.1	18 201.9	15 394.7	15 547.0	15 388.4	15 545.0
(1,16,0)Π	18 714.2 (11.0)	18 829.8 (8.7)	18 713.4 (10.9)	18 827.9 (7.7)	15 892.8 (26.2)	16 074.1 (38.2)	15 889.1 (22.0)	16 070.3 (33.4)
(1,17,0)Σ	19 333.5	19 477.8	19 332.6	19 476.4	16 312.8	16 557.0	16 311.5	16 552.3
(1,18,0)Π	19 913.3 (1.0)	20 037.2 (1.0)	19 911.9 (−0.5)	20 034.2 (1.2)	16 876.7 (11.3)	17 076.4 (18.7)	16 874.2 (8.7)	17 073.2 (16.0)

each vibronic band consists of a single feature with unresolved J substructure. The second panel shows a similar emission spectrum from $H^{11}BBr$ excited by the laser at 14 288 cm^{-1} in which each strong band has a weaker satellite feature (#1–#4) to higher wavenumbers. The intervals between the main bands and the satellites increase monotonically from 161 cm^{-1} (#1) to 223 cm^{-1} (#4). These intervals are much too small to be a vibrational frequency and we interpret them as transitions down to the $K = 3$ stack of levels in each bending state. The $K_a'' = 3 - K_a'' = 1$ interval in the (0,0,0) state is $\sim 8[A - (B + C)/2]$ which our *ab initio* results give as 161.8 cm^{-1}, increasing to 226.7 cm^{-1} for (0,3,0), both in very reasonable agreement with experiment. Most of the HBBr emission spectra from Σ upper states show these characteristic and unexpected $\Delta K = -3$ transitions. In fact, a close examination of the spectrum in the top panel in Fig. 3 shows that the same rotational satellites are present for most of the bands, although they are much weaker. Further confirmation of the assignment comes from a single, weak DBBr emission spectrum excited at 14 414 cm^{-1} which shows satellites of 93 and 95 cm^{-1} for the (0,0,0) and (0,1,0) lower states, in complete agreement with the *ab initio* values of 93.6 and 98.6 cm^{-1}.

The third panel in Fig. 3 shows an emission spectrum which originates from a $K = 1$ (Π) level of the upper state of $H^{11}BBr$. Each band consists of a closely spaced doublet which are the allowed transitions to the $K_a = 0$ and $K_a = 2$ stacks of rotational levels in each vibrational level of the ground state. The measured doublet down to the 0_0 level is 80 cm^{-1}, in good accord with the (0,0,0) value of 81.0 cm^{-1} obtained from our *ab initio* results. The bottom panel in Fig. 3 shows a weak emission spectrum from a similar Π level of $D^{11}BBr$ with a

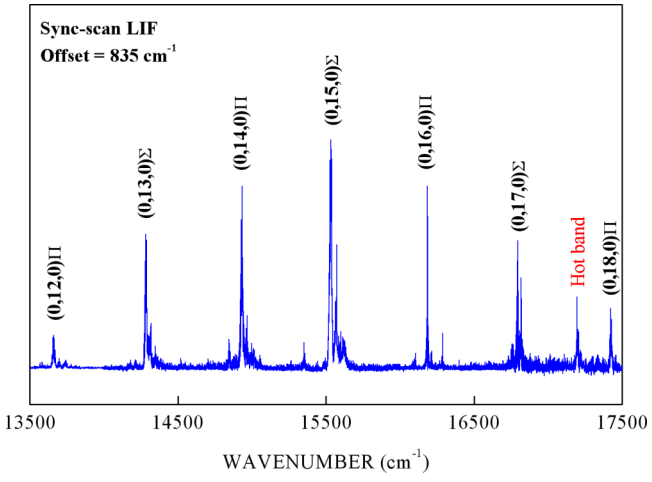

FIG. 2. A portion of the low-resolution sync-scan LIF spectrum of HBBr. The spectrum was recorded with a monochromator offset of 835 cm^{-1}, corresponding to the ground state bending fundamental of $H^{11}BBr$.

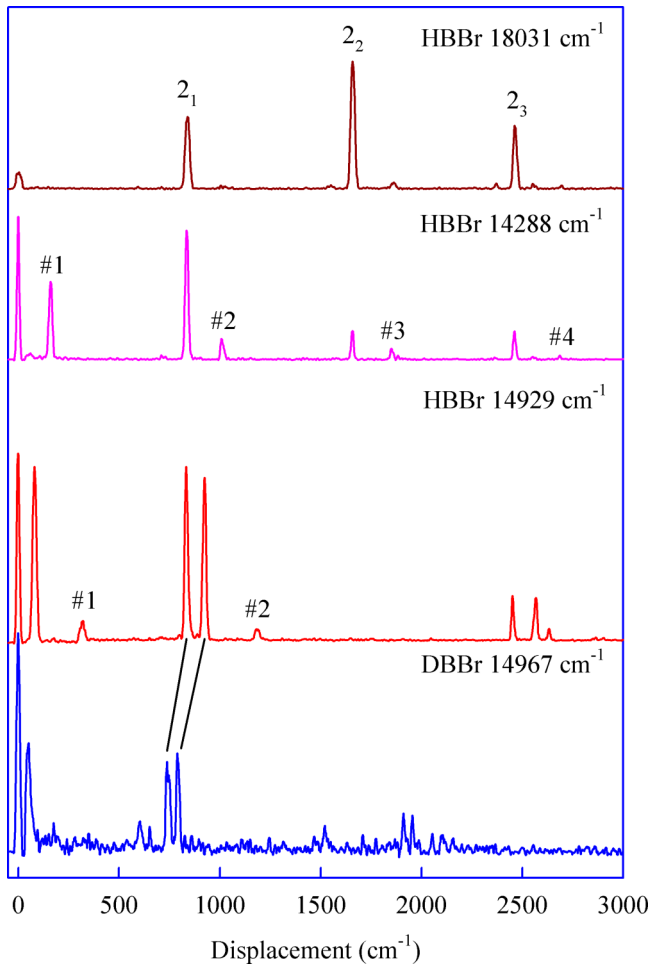

FIG. 3. Single vibronic level emission spectra of HBBr from a Σ upper vibronic state (top two panels) and a Π upper vibronic state (third panel) compared to that from DBBr (bottom) along with some ground state assignments. The wavenumber scale is displacement from the excitation laser position which gives a direct energy measure of the ground vibrational levels. The doublets that appear in the emission from Π upper states ($K = 1$) are due to emission down to $K_a = 0$ and $K_a = 2$ of each vibrational level in the ground state. The features labeled #1 - #4 are discussed in detail in the text.

doublet splitting of 44 cm^{-1}, precisely as expected due to the decrease in the A rotational constant on deuteration.

Returning to the third panel in Fig. 3, close inspection shows weak satellite bands (#1 and #2) with intervals of 318 and 353 cm^{-1} relative to the (0,0,0) and (0,1,0) $K_a = 0$ levels. Assuming that $\Delta K = \pm 3$ transitions can also occur for Π levels, we assign these features as transitions to $K_a = 4$ in the lower state, with a $K_a'' = 4 - K_a'' = 0$ interval of $\sim 16[A - (B + C)/2] \approx 320$ cm^{-1}. Similar $\Delta K = -3$ emission features were found for many, but not all, of the Π bands in the LIF spectrum of HBBr.

In addition to the prominent bending progressions in the emission spectra, there are also a few weak bands terminating on stretching or bend-stretch combination levels in the ground state, particularly in the spectra of DBBr. The measured energy levels and their assignments are summarized in Table IV.

In conclusion, we note that the upper state K value of each band in the LIF spectrum is in principle readily determinable by examining the corresponding emission spectrum for the presence or absence of doublets. In addition, the $\Delta K = -3$ transitions, if observed, provide confirmation of the K numbering in the upper state. These criteria were very useful in the analysis of the LIF spectra.

F. Assignment of the sync-scan LIF spectra

The LIF spectra were assigned by comparisons between observed and calculated transition frequencies and isotope shifts, and the upper state symmetries (Σ, Π *etc.*) determined (where possible) from the emission spectra. It is noteworthy that the symmetries alternate between Σ and Π across the major progression, indicating that the former have odd quanta and the latter even quanta of upper state bending quantum number, v_2', since $K = |l \pm 1|$ and the vibrational angular momentum quantum number $l = v_2, v_2 - 2, v_2 - 4, \ldots, 1$ or 0.

TABLE IV. Ground state energy levels (in cm^{-1}) and their assignments from the emission spectra of $H^{11}BBr$, $H^{10}BBr$, and $D^{11}BBr$ isotopologues.

Assignment	$H^{11}BBr$ Energy[a]	$H^{10}BBr$ Energy	$D^{11}BBr$ Energy
3_1	717 (718)	738 (741)	737 (742)
2_1	839 (838)	843 (849)	593 (599)
3_2	...	...	1466 (1476)
$2_1 3_1$	1550 (1555)	...	1330 (1334)
2_2	1661 (1661)	1671 (1683)	1191 (1196)
3_3	...	...	2184 (2200)
$2_1 3_2$	...	...	2050 (2061)
$2_2 3_1$	2370 (2377)	...	...
2_3	2463 (2466)	...	...
1_1	2553 (2559)	2565 (2570)	1907 (1910)
2_4	3248 (3252)	3275 (3295)	...
$1_1 2_1$	3383 (3391)	...	2492 (2500)
2_5	4015 (4018)	...	...

[a]Energy above the lowest vibrational level of the X^2A' state. The numbers in parentheses are calculated values for the corresponding ^{79}Br isotopologue from Table II.

TABLE V. Observed $\tilde{A}^2A'' - \tilde{X}^2A'$ transitions of $H^{11}BBr$ and $H^{10}BBr$ isotopologues (in cm^{-1}).

Upper state level	$H^{11}BBr$		$H^{11}BBr$ hot bands[c]		$H^{10}BBr$	
(v_1,v_2,v_3)	Obs.[a]	Obs. - calc.[b]	Obs.	Interval	Obs.	Obs. - calc.[b]
(0,10,0) Π	12 396.8	40.8	...	...	12 460.8	33.8
(0,12,0) Π[d]	13 582.8					
(0,12,0) Π	13 663.1	19.5	...	...	13 742.9	13.0
(1,8,0) Π	13 699.3	−5.9				
(0,13,0) Σ	14 287.8	37.9	...	...	...	...
(1,9,0) Σ	14 317.9	−12.7				
(0,14,0) Π[d]	14 846.0					
(0,14,0) Π	14 928.8	6.1	14 094.8	834.0	15 023.9	9.7
(1,10,0) Π	14 966.4	10.7				
(0,15,0) Σ	15 536.2	7.3	14 702.3	833.9	15 626.7	−0.1
(1,11,0) Σ	15 572.6	−7.8				
(0,16,0) Π[d]	16 104.7		...	...		
(0,16,0) Π	16 184.2	−1.4	15 350.9	833.3	16 288.3	−0.2
(1,12,0) Π	16 213.4	−16.6				
(0,17,0) Σ	16 794.5	7.9	15 960.6	833.9	16 879.5	−16.1
(1,13,0) Σ	16 818.1	−13.5				
(0,18,0) Π	17 427.5	−11.4	16 593.6	833.9	...	...
(1,14,0) Π	17 460.0	−17.3				
(0,19,0) Σ	18 030.9	−19.1	17 196.4	834.5	18 138.2	−33.7
(0,20,0) Π	18 664.5	−21.3	17 830.7	833.8	...	...
(0,21,0) Σ	19 256.6	−18.6	18 423.2	833.4		

[a]The Q-branch maximum of each band.
[b]The calculated values are taken from Table III. Calculated transitions to Σ upper states are corrected by subtracting the $1_{1,1}$ - $0_{0,0}$ interval, i.e., 21.4 cm^{-1} for $H^{11}BBr$ and 21.6 cm^{-1} for $H^{10}BBr$.
[c]Hot bands originate from the (0,1,0) ground state vibrational level.
[d]$K = 1 - K_a'' = 2$ transition.
[e]Very weak unassigned bands occur at 12 357, 14 181, 14 216, 16 732, and 16 764 cm^{-1}.

Our analysis began with the strong HBBr LIF band at 16 184.2 cm^{-1} [labeled (0,16,0)Π in Fig. 2]. Our experience with the spectra of the HBF and HBCl free radicals suggested that this band is most probably a transition from the ground state (0,0,0) level to a high bending level of the excited state. The emission spectrum clearly shows that the upper level is a Π state with $K = 1$ which dictates that v_2' = even. Examination of the calculated energy levels in Table III shows that the closest and most obvious candidate is (0,16,0) which is calculated (for the $H^{11}B^{79}Br$ isotopologue) to be only 1.4 cm^{-1} higher than observed. Shifting the upper state bending quantum number by ±2 would give offsets greater than 1000 cm^{-1} which appears unrealistically large for the present high level of theory.

Further evidence supporting this 2_0^{16} assignment comes from the observed and calculated isotope effects. According to the data in Table III, there should be a transition to (0,16,0) of $H^{10}BBr \sim 103$ cm^{-1} to higher energy and the corresponding bands of $D^{11}BBr$ and $D^{10}BBr$ should appear 2244 and 2092 cm^{-1} below that of $H^{11}BBr$. The isotope shifts of the alternative (0,14,0) and (0,18,0) assignments are substantially different and readily distinguished from those of (0,16,0). Experimentally, the isotopologue transitions were located with offsets of +104.1, −2217, and −2055 cm^{-1}, respectively, providing strong validation of the initial (0,16,0) identification.

The strong bands immediately above and below 2_0^{16} were then immediately assignable as members of the bending progression. The upper state symmetries, determined from the emission spectra, alternate between Σ and Π as expected and the obs-calc values range, for $H^{11}BBr$ and $H^{10}BBr$, from +41 to −34 cm^{-1}. The obs-calc values tend to decrease with increasing energy, indicating that the *ab initio* surface is somewhat flatter than required. The calculated isotope shifts allowed us to identify several weak bands 50–100 cm^{-1} above the stronger $H^{11}BBr$ features which were assigned to $H^{10}BBr$ (see Fig. 2). In addition, a series of weak bands ~833 cm^{-1} below the main progression (Fig. 2) proved to be hot bands originating from the (0,1,0) level in the ground state. We also noted that a few of the Π bands had a corresponding weak satellite transition approximately 80 cm^{-1} to lower energy (Fig. 2), whose emission spectra (where available) were identical to that of the stronger analogues. These were proven to be the much weaker $K' = 1 - K_a'' = 2$ counterparts of the $K' = 1 - K_a'' = 0$ transitions. The efficient cooling in the supersonic expansion substantially depopulates the ground state $K_a = 2$ levels; so, transitions from them are only rarely observed in our spectra.

Most of the strong Σ and Π bands in the $H^{11}BBr$ spectrum have a satellite 20–40 cm^{-1} to higher energy that proved difficult to assign. The emission spectra of the 2_0^{12}, 2_0^{13}, 2_0^{15}, 2_0^{17} band satellites were recorded and found to have the same features with the same relative intensities as those of the parent bands, but the emission bands were shifted 20–40 cm^{-1} higher in energy. To explain these bands, we first considered the possibility that they were due either to different spin components of the main bands (for Π states only) or to higher angular momentum components (i.e., Δ and Φ components of the same bending level). However, the spin-orbit splittings of the Π states were predicted to be small and with randomly distributed signs (see Table III), while the higher angular momentum components were calculated to fall either lower or at nearly equal energies with respect to the pure bending levels.

We then turned our attention to other explanations. Looking at Table III, it is evident that for the $H^{11}B^{79}Br$ isotopologue, the $(1,v_2-4,0)$ transitions always fall within 30-50 cm^{-1} above the corresponding $(0,v_2,0)$ levels. These are good candidates for the assignment of the weak satellite bands, since the symmetries of the $(1,v_2-4,0)$ and $(0,v_2,0)$ levels are the same, so they can mix through a higher order Fermi resonance mechanism. The existence of mixing between these levels is confirmed by the composition of the wavefunction vector in the variational computations.

A different explanation is required for the unexpected $\Delta K = 3$ transitions observed in the emission spectra. As stated in Section III E, the $\Delta K = \pm 1$ selection rule implies that "pure" Σ levels ($K' = 0$) of the $\tilde{A}^2A''$ electronic would emit back only to $K'' = 1$ ($\Delta K = +1$) of the $\tilde{X}^2A'$ ground state, while "pure" Π levels ($K' = 1$) would emit down to $K'' = 0$ ($\Delta K = -1$) and $K'' = 2$ ($\Delta K = +1$) levels. However, the complete Renner-Teller spin-rovibronic Hamiltonian of Carter *et al.*[17] allows for a mixing of rotational levels of the same electronic state with $\Delta K = \pm 1$ and $\Delta K = \pm 2$. This means that Σ and Π levels of $\tilde{A}^2A''$ may have partial Δ and Φ character, respectively. Hence, "mixed" Σ levels can emit to $K'' = 3$ and "mixed" Π levels can emit to $K'' = 4$. In such cases, $\Delta K = 3$ transitions would be expected and that is what is observed. The complete set of assignments for HBBr are summarized in Table V.

TABLE VI. Observed $\tilde{A}^2A''-\tilde{X}^2A'$ transitions of DBBr (in cm^{-1}).

	$D^{11}BBr$		$D^{10}BBr$	
(v_1,v_2,v_3)	Obs.[a]	Obs. - calc.[b]	Obs.	Obs. - calc.
(0,12,0) Π	11 958.2	45.6	12 069.5	46.7
(0,14,0) Π[c]	12 927.7			
(0,14,0) Π	12 965.4	33.1	13 099.9	36.2
(1,11,0) Σ	13 425	39.3		
(0,15,0) Σ	13 460.4	30.5	…	…
(0,16,0) Π[c]	13 918.3			
(1,12,0) Π	13 940	50.2		
(0,16,0) Π	13 967.2	25.6	14 126.0	32.7
(1,13,0) Σ	14 413	30.2		
(0,17,0) Σ	14 460.9	31.3	…	…
(0,18,0)Π[c]	14 911.7			
(1,14,0) Π	14 885	9.3		
(0,18,0) Π	14 962.5	14.0	…	…
(1,15,0) Σ	15 395	12.9		
(0,19,0) Σ	15 450.1	20.4	…	…
(1,16,0) Π	15 901	8.2		
(0,20,0) Π	15 960.8	11.1	16 147.6	5.7
(0,21,0) Σ	16 433.0	7.8	…	…

[a]The Q-branch maximum of each band.
[b]The calculated values are taken from our theoretical study listed in TABLE III. Calculated transitions to Σ upper states are corrected by subtracting the $1_{1,1}$ - $0_{0,0}$ interval, i.e., 12.6 cm^{-1} for $D^{11}BBr$ and 13.0 cm^{-1} for $D^{10}BBr$.
[c]$K = 1 - K_a'' = 2$ transition.
[d]Weak unassigned bands occur at 13 142, 13 443, 13 666, 13 781, 15 078, 15 318, 15 553, and 16 148 cm^{-1}.

The LIF spectra of DBBr were much weaker and noisier than those of HBBr and hampered our ability to obtain emission spectra, so the analysis is necessarily less complete. Nevertheless, the main bending progression of $D^{11}BBr$ bands with alternating Σ and Π upper state symmetries was readily identifiable based on the comparison of observed and calculated transition frequencies, deuterium isotope shifts and K' quantum numbers from emission spectra (where available). As in the HBBr case, some of the DBBr transitions to Π states showed a weak transition ~40 cm^{-1} to lower energy which was assigned at the corresponding $K = 1 - K''_a = 2$ transition. In addition, in favorable cases, the weak $D^{10}BBr$ bands were found 135 – 200 cm^{-1} above the main $D^{11}BBr$ bending progression. Finally we see the same kind of Fermi resonances in $D^{11}B^{79}Br$ as were found in HBBr, but in this case the $(1,v_2 - 4,0)$ transitions fall approximately 50 cm^{-1} below the $(0,v_2,0)$ levels. Many weak bands in the $D^{11}BBr$ spectrum were assigned in this way. All of the measured bands and the assignments, where available, are reported in Table VI.

IV. DISCUSSION

A. The molecular structure of HBBr

As in previous work on HBCl, we were unable to obtain high-resolution spectra of HBBr or DBBr for the determination of molecular structures, so must depend on the results of our *ab initio* calculations. The best structures, which come from the potential energy surfaces, are r_{BH} = 1.186 Å, r_{BBr} = 1.863 Å, and θ = 123.5° for the bent ground state and r_{BH} = 1.166 Å, r_{BBr} = 1.824 Å for the linear excited state. These values are compared to the geometric parameters derived from *ab initio* potential energy surfaces for HBF, HBCl, and BH_2 in Table VII.

The ground state bond length of diatomic BBr (1.887 Å) is 0.024 Å longer than that of HBBr (1.863 Å), and their B—Br stretching vibrational frequencies of 685.2 and 717 cm^{-1}, respectively, are in accord with the bond lengths.[37]

TABLE VII. Comparison of the ground and excited state *ab initio* molecular structures and barriers to linearity of the HBX (X = F, Cl, Br, H) free radicals.

Parameter	HBF[a]	HBCl[b]	HBBr[c]	BH_2[d]
r'' (BH) Å	1.203	1.190	1.186	1.188
r'' (BX) Å	1.309	1.716	1.863	1.188
θ″ (°)	121.1	123.4	123.5	129.0
r' (BH) Å	1.167	1.166	1.166	1.170
r' (BX) Å	1.307	1.681	1.824	1.170
θ′ (°)	180	180	180	180
Barrier to linearity (cm^{-1})	10 084	6 073	5 607	2 743
First excited $A'(\Sigma)$ state at linearity (cm^{-1})[e]	17 590	26 188	25 990	40 019

[a]Reference 14.
[b]Reference 16.
[c]This work.
[d]Reference 39.
[e]Calculated at the $A''(\Pi)$ excited state equilibrium geometry reported above. The energy of the first excited $A'(\Sigma)$ electronic state has been evaluated with Molpro at the state-averaged CASSCF level, using the cc-pVTZ basis for all molecules.

The ground state BH bond lengths of the various radicals in Table VII decrease in going from fluorine to bromine, and the bond length of HBBr is almost identical to that of BH_2. Viewing these molecules as BX (X = F, Cl, Br, H) diatomics with an added hydrogen, it is apparent that the ground state BH bond lengths get longer and the bond angles get smaller with the increasing electronegativity of the X atom.

There is a consistent trend that all the bond lengths decrease on electronic excitation (Table VII), as would be expected for excitation from an in-plane antibonding π orbital (HOMO) to the LUMO which is predominantly an out-of-plane $2p_z$ nonbonding orbital localized on the boron atom. Of course, in all the cases, the radical adopts a linear geometry on electronic excitation, in accord with the expectations from Walsh diagrams.

There is a regular trend in the barriers to linearity, ranging from ~2700 cm^{-1} for BH_2[39] to more than 10 000 cm^{-1} for HBF. Our presumption is that the lower A' component of the ground state is vibronically coupled with a higher excited state of Σ symmetry through the π bending vibration.[40,41] To test this hypothesis, we performed some trial computations of the electronic structure of these radicals, using the Complete Active Space Self Consistent Field (CASSCF) method. In particular, we estimated the energy of the closest excited state above the ground state at linear geometries (see Table VII). We found that at linearity the first excited state is always a $\Sigma(A')$ state, which has the right symmetry to interact, upon bending, with the A' component of the ground electronic Π state. The energy of the Σ state increases regularly from HBF(≈17 500 cm^{-1}), to HBCl and HBBr (≈26 000 cm^{-1}), to BH_2 (≈40 000 cm^{-1}). The splitting of the ground state and its stabilization to a bent configuration can then be attributed to a strong vibronic interaction with the Σ state. The closer is the Σ state, the larger is the interaction and the deeper the energy well, with a consequent increase of the barrier to linearity.

B. Agreement between theory and experiment

The data in Table IV show that there is excellent agreement between the observed and calculated ground state energy levels for all three isotopologues of HBBr, with differences typically of the order of the experimental error (±2-3 cm^{-1}) in many cases. All three fundamentals are predicted within a few cm^{-1} of experiment and the calculations even reproduce the location of the highest observed bending level (v_2 = 5 of $H^{11}BBr$ at 4015 cm^{-1}) within 3 cm^{-1} of the experimental value. It is apparent that the ground state potential is quite reliable over the data range of our emission observations.

As discussed previously, we have empirically adjusted the HBBr excited state potential downwards by 98 cm^{-1} in order to provide a better comparison with the experimentally observed bending levels. A mismatch between experiment and calculation of about 100 cm^{-1} is precisely what was found in our previous studies of HBF[14] and HBCl[16] and normally would not be cause for concern. However, the spectra of HBBr were more complex than previous studies and so we elected to adjust the potentials to provide the best possible match

between the main observed bands and calculated values. As can be seen from the obs-calc values in Tables V and VI, the resulting agreement is very good for the four observed isotopologues. It is obvious from Tables II and III that the bromine isotope splittings are expected to be a few cm^{-1} at most, and would be buried in the rotational contours of the LIF bands, accounting for our inability to identify them in the spectra.

The calculated spin-orbit splittings for the HBX radicals are HBF^{14} = 42.3 cm^{-1}, $HBCl^{16}$ = 87.3 cm^{-1}, and HBBr = 299.7 cm^{-1}. These can be compared to the known ground state ($^2\Pi_r$) spin-orbit constants of the isoelectronic CX diatomic radicals[42] which have values of CF = 77 cm^{-1}, CCl = 135 cm^{-1}, and CBr = 466 cm^{-1}. Clearly, there is a strong correlation, with the HBX *ab initio* predictions which are always lower than the CX experimental values by 35%–45%.

It is apparent from the calculations and the observed spectra that transitions to the (1, v_2 – 4, 0) levels gain intensity by Fermi resonance mixing with the (0,v_2,0) levels of the same symmetry. Our observation that the $H^{11}BBr$ emission spectra from both members of a limited number of such Fermi resonance coupled levels are very similar suggests that the majority of the intensity derives from the transition to the pure bending levels. The situation is less clear for DBBr, as the spectra were too weak to record emission spectra from the satellite bands, but we envision that the mechanism must be similar.

Our observations of emission transitions involving changes in the K quantum number by 3 are unusual, as such anomalies were not observed in our previous studies of the spectra of HBF and HBCl. However, they are not unprecedented. For example, in BH_2, Herzberg and Johns[38] found clear evidence for K-type resonance (a type of Coriolis interaction) between the nearby Σ and Δ components of the (0,13,0) excited state level. Such mixing will induce some K = 2 (Δ) character into the K = 0 (Σ) level and could give rise to anomalous fluorescence of the type we see in HBBr. The fact that the HBBr calculated Σ – Δ and Π – Φ splittings of a given bending level are quite small probably accounts for the observed mixing, which must also be quite limited since the ΔK = 3 emission bands are weak.

V. CONCLUSIONS

This paper concludes our in-depth experimental and computational studies of the HBF, HBCl, and HBBr free radicals that the Clouthier group at the University of Kentucky discovered a decade ago.[13] In each case, the observed band system in the visible involves a linear-bent transition between the two Renner-Teller components of what would be a $^2\Pi$ state at linearity. As a consequence, the bands terminate on high bending levels of the excited state and the 0—0 band is both weak and undetectable by conventional laser-induced fluorescence techniques. As a result, it was difficult to make vibronic assignments purely from the experimental data and the quest for computational help spawned a very productive collaboration between the experimentalists at Kentucky and the computational group of Riccardo Tarroni at the University of Bologna in Italy. The *ab initio* computation of high-quality potential energy surfaces and the subsequent variational calculation of the rovibronic energy levels proved crucial to a detailed understanding of these spectra and the theoretical results made it possible to arrive at unambiguous assignments. In fact, in our recent foray into the spectroscopy of BH_2,[39] we have shown that it is possible to calculate the rovibronic energy levels of this seven electron free radical to near spectroscopic accuracy (within a few cm^{-1}) at energies as high as 22 000 cm^{-1} above the ground state zero-point level, without the necessity for any empirical adjustments of the potential.[39] The marriage of experiment and theory has proven to be a powerful combination for the detailed study of these complex free radical spectra.

ACKNOWLEDGMENTS

This material is based upon work supported by the National Science Foundation under Grant No. CHE-1106338. R.T. acknowledges financial support from the University of Bologna.

[1]O. Sezer and J. I. Brand, Mater. Sci. Eng. B **79**, 191 (2001).
[2]M. D. Allendorf and C. F. Melius, J. Phys. Chem. A **101**, 2670 (1997), and references therein.
[3]R. Naslain, J. Thebault, and P. Hagenmuller, J. Less-Common Met. **67**, 85 (1979).
[4]V. Cholet, R. Herbin, and L. Vandenbulcke, Thin Solid Films **188**, 143 (1990).
[5]B. J. Choi, D. W. Park, and D. R. Kim, J. Mater. Sci. Lett. **14**, 452 (1995).
[6]N. A. Sezgi, T. Dogu, and H. O. Ozbelge, Chem. Eng. Sci. **54**, 3297 (1999).
[7]N. A. Sezgi, A. Ersoy, T. Dogu, and H. O. Ozbelge, Chem. Eng. Process. **40**, 525 (2001).
[8]J. Berjonneau, G. Chollon, and F. Langlais, J. Electrchem. Soc. **153**, C795 (2006).
[9]H. B. Schlegel and S. J. Harris, J. Phys. Chem. **98**, 11178 (1994).
[10]H. B. Schlegel, A. G. Baboul, and S. J. Harris, J. Phys. Chem. **100**, 9774 (1996).
[11]Y. Zeng, K. Su, J. Deng, T. Wang, Q. Zeng, L. Cheng, and L. Zhang, J. Mol. Struct: Theochem. **861**, 103 (2008).
[12]S. J. Harris, J. Kiefer, Q. Zhang, A. Schoene, and K.-W. Lee, J. Electrochem. Soc. **145**, 3203 (1998).
[13]S.-G. He, F. X. Sunahori, and D. J. Clouthier, J. Am. Chem. Soc. **127**, 10814 (2005).
[14]F. X. Sunahori, D. J. Clouthier, S. Carter, and R. Tarroni, J. Chem. Phys. **130**, 164309 (2009).
[15]F. X. Sunahori and D. J. Clouthier, J. Chem. Phys. **130**, 164310 (2008).
[16]M. Gharaibeh, D. J. Clouthier, and R. Tarroni, J. Chem. Phys. **142**, 014305 (2015).
[17]S. Carter, N. C. Handy, P. Rosmus, and G. Chambaud, Mol. Phys. **71**, 605 (1990).
[18]S. Carter, N. C. Handy, C. Puzzarini, R. Tarroni, and P. Palmieri, Mol. Phys. **98**, 1697 (2000).
[19]H. Harjanto, W. W. Harper, and D. J. Clouthier, J. Chem. Phys. **105**, 10189 (1996).
[20]W. W. Harper and D. J. Clouthier, J. Chem. Phys. **106**, 9461 (1997).
[21]D. L. Michalopoulos, M. E. Geusic, P. R. R. Langridge-Smith, and R. E. Smalley, J. Chem. Phys. **80**, 3556 (1984).
[22]J. Yang and D. J. Clouthier, J. Chem. Phys. **135**, 054309 (2011).
[23]M. J. Frisch, G. W. Trucks, H. B. Schlegel *et al.*, GAUSSIAN 03, Revision C.02, Gaussian, Inc., Wallingford, CT, 2004.
[24]A. D. Becke, J. Chem. Phys. **98**, 5648 (1993).
[25]C. Lee, W. Yang, and R. G. Parr, Phy. Rev. B **37**, 785 (1988).
[26]K. Raghavachari, G. W. Trucks, J. A. Pople, and M. Head-Gordon, Chem. Phys. Lett. **157**, 479 (1989).
[27]T. H. Dunning, Jr., J. Chem. Phys. **90**, 1007 (1989).
[28]K. Dressler and D. A. Ramsay, Philos. Trans. R. Soc., A **251**, 553 (1959).
[29]K. A. Peterson, B. A. Flowers, and J. S. Francisco, J. Chem. Phys. **115**, 7513 (2001).

[30]CFOUR, a quantum-chemical program package by, J. F. Stanton, J. Gauss, M. E. Harding, P. G. Szalay, with contributions from, A. A. Auer, R. J. Bartlett, U. Benedikt, C. Berger, D. E. Bernholdt, Y. J. Bomble, L. Cheng, O. Christiansen, M. Heckert, O. Heun, C. Huber, T.-C. Jagau, D. Jonsson, J. Jusélius, K. Klein, W. J. Lauderdale, D. A. Matthews, T. Metzroth, L. A. Mück, D. P. O'Neill, D. R. Price, E. Prochnow, C. Puzzarini, K. Ruud, F. Schiffmann, W. Schwalbach, S. Stopkowicz, A. Tajti, J. Vázquez, F. Wang, J. D. Watts, the integral packages MOLECULE (J. Almlöf P. R. Taylor), PROPS (P. R. Taylor), ABACUS (T. Helgaker, H. J. Aa. Jensen, P. Jørgensen, and J. Olsen), and ECP routines by, A. V. Mitin, and C. van Wüllen, For the current version, 2010, see http://www.cfour.de.

[31]K. A. Peterson and T. H. Dunning, Jr., J. Chem. Phys. **117**, 10548 (2002).

[32]K. A. Peterson and K. E. Yousaf, J. Chem. Phys. **133**, 174116 (2010).

[33]J. Senekowitsch, Ph.D. thesis (Johann Wolfgang Goethe Universität, Frankfurt am Main, Germany, 1988).

[34]See supplementary material at http://dx.doi.org/10.1063/1.4953771 for a table of the expansion coefficients of the HBBr potential energy surfaces. This document can be reached via a direct link in the article's HTML reference section or via the EPAPS homepage http://www.aip.org/pubservs/epaps.html.

[35]H.-J. Werner, P. J. Knowles, F. R. Manby, M. Schütz, P. Celani, G. Knizia, T. Korona, R. Lindh, A. Mitrushenkov, G. Rauhut, T. B. Adler, R. D. Amos, A. Bernhardsson, A. Berning, D. L. Cooper, M. J. O. Deegan, A. J. Dobbyn, F. Eckert, E. Goll, C. Hampel, A. Hesselmann, G. Hetzer, T. Hrenar, G. Jansen, C. Köppl, Y. Liu, A. W. Lloyd, R. A. Mata, A. J. May, S. J. McNicholas, W. Meyer, M. E. Mura, A. Nicklass, P. Palmieri, K. Pflüger, R. Pitzer, M. Reiher, T. Shiozaki, H. Stoll, A. J. Stone, R. Tarroni, T. Thorsteinsson, M. Wang, and A. Wolf, MOLPRO, version 2010.1, a package of *ab initio* programs, 2010, see http://www.molpro.net.

[36]A. O. Mitrushchenkov, J. Chem. Phys. **136**, 024108 (2012).

[37]N. T. Hunt, W. Y. Fan, Z. Liu, and P. B. Davies, J. Mol. Spectrosc. **191**, 326 (1998), and references therein.

[38]G. Herzberg and J. W. C. Johns, Proc. R. Soc. London, Ser. A **298**, 142 (1967).

[39]F. X. Sunahori, M. Gharaibeh, D. J. Clouthier, and R. Tarroni, J. Chem. Phys. **142**, 174302 (2015).

[40]The details of this type of vibronic coupling are thoroughly discussed in, A. G. Adam, K. Athanassenas, D. A. Gillett, C. T. Kingston, A. J. Merer, J. R. D. Peers, and S. J. Rixon, J. Mol. Spectrosc. **196**, 45 (1999).

[41]P. Garcia-Fernandez and I. B. Bersuker, Int. J. Quantum Chem. **112**, 3025 (2012).

[42]K. Huber and G. Herzberg, *Molecular Spectra and Molecular Structure. IV. Constants of Diatomic Molecules* (Van Nostrand Reinhold Company, New York, 1979).